FERMILAB-PUB-20-127-ND-PPD-TD
ACCEPTED

A Three Year Sample of Almost 1600 Elves Recorded Above South America by the Pierre Auger Cosmic-Ray Observatory

A. Aab[75], P. Abreu[67], M. Aglietta[50,49], I.F.M. Albuquerque[19], J.M. Albury[12], I. Allekotte[1], A. Almela[8,11], J. Alvarez Castillo[63], J. Alvarez-Muñiz[74], G.A. Anastasi[42,43], L. Anchordoqui[82], B. Andrada[8], S. Andringa[67], C. Aramo[47], H. Asorey[1,28], P. Assis[67], G. Avila[9,10], A.M. Badescu[70], A. Bakalova[30], A. Balaceanu[68], F. Barbato[56,47], R.J. Barreira Luz[67], S. Baur[37], K.H. Becker[35], J.A. Bellido[12], C. Berat[34], M.E. Bertaina[58,49], X. Bertou[1], P.L. Biermann[1001], J. Biteau[32], S.G. Blaess[12], A. Blanco[67], J. Blazek[30], C. Bleve[52,45], M. Boháčová[30], D. Boncioli[42,43], C. Bonifazi[24], N. Borodai[64], A.M. Botti[8,37], J. Brack[1004], T. Bretz[39], A. Bridgeman[36], F.L. Briechle[39], P. Buchholz[41], A. Bueno[73], S. Buitink[14], M. Buscemi[54,44], K.S. Caballero-Mora[62], L. Caccianiga[55], L. Calcagni[4], A. Cancio[11,8], F. Canfora[75,77], J.M. Carceller[73], R. Caruso[54,44], A. Castellina[50,49], F. Catalani[17], G. Cataldi[45], L. Cazon[67], M. Cerda[9], J.A. Chinellato[20], J. Chudoba[30], L. Chytka[31], R.W. Clay[12], A.C. Cobos Cerutti[7], R. Colalillo[56,47], A. Coleman[86], M.R. Coluccia[52,45], R. Conceição[67], A. Condorelli[42,43], G. Consolati[46,51], F. Contreras[9,10], M.J. Cooper[12], S. Coutu[86], C.E. Covault[80], B. Daniel[20], S. Dasso[5,3], K. Daumiller[37], B.R. Dawson[12], J.A. Day[12], R.M. de Almeida[26], S.J. de Jong[75,77], G. De Mauro[75,77], J.R.T. de Mello Neto[24,25], I. De Mitri[42,43], J. de Oliveira[26], F.O. de Oliveira Salles[15], V. de Souza[18], J. Debatin[36], M. del Río[10], O. Deligny[32], N. Dhital[64], M.L. Díaz Castro[20], F. Diogo[67], C. Dobrigkeit[20], J.C. D'Olivo[63], Q. Dorosti[41], R.C. dos Anjos[23], M.T. Dova[4], A. Dundovic[40], J. Ebr[30], R. Engel[36,37], M. Erdmann[39], C.O. Escobar[1002], A. Etchegoyen[8,11], H. Falcke[75,78,77], J. Farmer[87], G. Farrar[85], A.C. Fauth[20], N. Fazzini[1002], F. Feldbusch[38], F. Fenu[58,49], L.P. Ferreyro[8], J.M. Figueira[8], A. Filipčič[72,71], M.M. Freire[6], T. Fujii[87,1005], A. Fuster[8,11], B. García[7], H. Gemmeke[38], A. Gherghel-Lascu[68], P.L. Ghia[32], U. Giaccari[15], M. Giammarchi[46], M. Giller[65], D. Głas[66], J. Glombitza[39], F. Gobbi[9], G. Golup[1], M. Gómez Berisso[1], P.F. Gómez Vitale[9,10], J.P. Gongora[9], N. González[8], I. Goos[1,37], D. Góra[64], A. Gorgi[50,49], M. Gottowik[35], T.D. Grubb[12], F. Guarino[56,47], G.P. Guedes[21], E. Guido[49,58], R. Halliday[80], M.R. Hampel[8], P. Hansen[4], D. Harari[1], T.A. Harrison[12], V.M. Harvey[12], A. Haungs[37], T. Hebbeker[39], D. Heck[37], P. Heimann[41], G.C. Hill[12], C. Hojvat[1002], E.M. Holt[36,8], P. Homola[64], J.R. Hörandel[75,77], P. Horvath[31], M. Hrabovský[31], T. Huege[37,14], J. Hulsman[8,37], A. Insolia[54,44], P.G. Isar[69], I. Jandt[35], J.A. Johnsen[81], M. Josebachuili[8], J. Jurysek[30], A. Kääpä[35], K.H. Kampert[35], B. Keilhauer[37], N. Kemmerich[19], J. Kemp[39],

This document was prepared by Pierre Auger collaboration using the resources of the Fermi National Accelerator Laboratory (Fermilab), a U.S. Department of Energy, Office of Science, HEP User Facility. Fermilab is managed by Fermi Research Alliance, LLC (FRA), acting under Contract No. DE-AC02-07CH11359.

H.O. Klages[37], M. Kleifges[38], J. Kleinfeller[9], R. Krause[39], D. Kuempel[35], G. Kukec Mezek[71], A. Kuotb Awad[36], B.L. Lago[16], D. LaHurd[80], R.G. Lang[18], R. Legumina[65], M.A. Leigui de Oliveira[22], V. Lenok[37], A. Letessier-Selvon[33], I. Lhenry-Yvon[32], O.C. Lippmann[15], D. Lo Presti[54,44], L. Lopes[67], R. López[59], A. López Casado[74], R. Lorek[80], Q. Luce[32], A. Lucero[8], M. Malacari[87], G. Mancarella[52,45], D. Mandat[30], B.C. Manning[12], P. Mantsch[1002], A.G. Mariazzi[4], I.C. Mariş[13], G. Marsella[52,45], D. Martello[52,45], H. Martinez[60], O. Martínez Bravo[59], M. Mastrodicasa[53,43], H.J. Mathes[37], S. Mathys[35], J. Matthews[83], G. Matthiae[57,48], E. Mayotte[35], P.O. Mazur[1002], G. Medina-Tanco[63], D. Melo[8], A. Menshikov[38], K.-D. Merenda[81], S. Michal[31], M.I. Micheletti[6], L. Middendorf[39], L. Miramonti[55,46], B. Mitrica[68], D. Mockler[36], S. Mollerach[1], F. Montanet[34], C. Morello[50,49], G. Morlino[42,43], M. Mostafá[86], A.L. Müller[8,37], M.A. Muller[20,1003], S. Müller[36,8], R. Mussa[49], L. Nellen[63], P.H. Nguyen[12], M. Niculescu-Oglinzanu[68], M. Niechciol[41], D. Nitz[84,1006], D. Nosek[29], V. Novotny[29], L. Nožka[31], A Nucita[52,45], L.A. Núñez[28], A. Olinto[87], M. Palatka[30], J. Pallotta[2], M.P. Panetta[52,45], P. Papenbreer[35], G. Parente[74], A. Parra[59], M. Pech[30], F. Pedreira[74], J. Pękala[64], R. Pelayo[61], J. Peña-Rodriguez[28], L.A.S. Pereira[20], M. Perlin[8], L. Perrone[52,45], C. Peters[39], S. Petrera[42,43], J. Phuntsok[86], T. Pierog[37], M. Pimenta[67], V. Pirronello[54,44], M. Platino[8], J. Poh[87], B. Pont[75], C. Porowski[64], R.R. Prado[18], P. Privitera[87], M. Prouza[30], A. Puyleart[84], S. Querchfeld[35], S. Quinn[80], R. Ramos-Pollan[28], J. Rautenberg[35], D. Ravignani[8], M. Reininghaus[37], J. Ridky[30], F. Riehn[67], M. Risse[41], P. Ristori[2], V. Rizi[53,43], W. Rodrigues de Carvalho[19], J. Rodriguez Rojo[9], M.J. Roncoroni[8], M. Roth[37], E. Roulet[1], A.C. Rovero[5], P. Ruehl[41], S.J. Saffi[12], A. Saftoiu[68], F. Salamida[53,43], H. Salazar[59], G. Salina[48], J.D. Sanabria Gomez[28], F. Sánchez[8], E.M. Santos[19], E. Santos[30], F. Sarazin[81], R. Sarmento[67], C. Sarmiento-Cano[8], R. Sato[9], P. Savina[52,45], M. Schauer[35], V. Scherini[45], H. Schieler[37], M. Schimassek[36], M. Schimp[35], F. Schlüter[37], D. Schmidt[36], O. Scholten[76,14], P. Schovánek[30], F.G. Schröder[88,37], S. Schröder[35], J. Schumacher[39], S.J. Sciutto[4], M. Scornavacche[8], R.C. Shellard[15], G. Sigl[40], G. Silli[8,37], O. Sima[68,1007], R. Šmída[87], G.R. Snow[89], P. Sommers[86], J.F. Soriano[82], J. Souchard[34], R. Squartini[9], D. Stanca[68], S. Stanič[71], J. Stasielak[64], P. Stassi[34], M. Stolpovskiy[34], A. Streich[36], F. Suarez[8,11], M. Suárez-Durán[28], T. Sudholz[12], T. Suomijärvi[32], A.D. Supanitsky[8], J. Šupík[31], Z. Szadkowski[66], A. Taboada[37], O.A. Taborda[1], A. Tapia[27], C. Timmermans[77,75], C.J. Todero Peixoto[17], B. Tomé[67], G. Torralba Elipe[74], A. Travaini[9], P. Travnicek[30], M. Trini[71], M. Tueros[4], R. Ulrich[37], M. Unger[37], M. Urban[39], J.F. Valdés Galicia[63], I. Valiño[42,43], L. Valore[56,47], P. van Bodegom[12], A.M. van den Berg[76], A. van Vliet[75], E. Varela[59], B. Vargas Cárdenas[63],

D. Veberič[37], C. Ventura[25], I.D. Vergara Quispe[4], V. Verzi[48], J. Vicha[30], L. Villaseñor[59], J. Vink[79], S. Vorobiov[71], H. Wahlberg[4], A.A. Watson[1000], M. Weber[38], A. Weindl[37], M. Wiedeński[66], L. Wiencke[81], H. Wilczyński[64], T. Winchen[14], M. Wirtz[39], D. Wittkowski[35], B. Wundheiler[8], L. Yang[71], A. Yushkov[30], E. Zas[74], D. Zavrtanik[71,72], M. Zavrtanik[72,71], L. Zehrer[71], A. Zepeda[60], B. Zimmermann[37], M. Ziolkowski[41], Z. Zong[32], F. Zuccarello[54,44]

[1]Centro Atómico Bariloche and Instituto Balseiro (CNEA-UNCuyo-CONICET), San Carlos de Bariloche, Argentina

[2]Centro de Investigaciones en Láseres y Aplicaciones, CITEDEF and CONICET, Villa Martelli, Argentina

[3]Departamento de Física and Departamento de Ciencias de la Atmósfera y los Océanos, FCEyN, Universidad de Buenos Aires and CONICET, Buenos Aires, Argentina

[4]IFLP, Universidad Nacional de La Plata and CONICET, La Plata, Argentina

[5]Instituto de Astronomía y Física del Espacio (IAFE, CONICET-UBA), Buenos Aires, Argentina

[6]Instituto de Física de Rosario (IFIR) – CONICET/U.N.R. and Facultad de Ciencias Bioquímicas y Farmacéuticas U.N.R., Rosario, Argentina

[7]Instituto de Tecnologías en Detección y Astropartículas (CNEA, CONICET, UNSAM), and Universidad Tecnológica Nacional – Facultad Regional Mendoza (CONICET/CNEA), Mendoza, Argentina

[8]Instituto de Tecnologías en Detección y Astropartículas (CNEA, CONICET, UNSAM), Buenos Aires, Argentina

[9]Observatorio Pierre Auger, Malargüe, Argentina

[10]Observatorio Pierre Auger and Comisión Nacional de Energía Atómica, Malargüe, Argentina

[11]Universidad Tecnológica Nacional – Facultad Regional Buenos Aires, Buenos Aires, Argentina

[12]University of Adelaide, Adelaide, S.A., Australia

[13]Université Libre de Bruxelles (ULB), Brussels, Belgium

[14]Vrije Universiteit Brussels, Brussels, Belgium

[15]Centro Brasileiro de Pesquisas Fisicas, Rio de Janeiro, RJ, Brazil

[16]Centro Federal de Educação Tecnológica Celso Suckow da Fonseca, Nova Friburgo, Brazil

[17]Universidade de São Paulo, Escola de Engenharia de Lorena, Lorena, SP, Brazil

[18]Universidade de São Paulo, Instituto de Física de São Carlos, São Carlos, SP, Brazil

[19]Universidade de São Paulo, Instituto de Física, São Paulo, SP, Brazil

[20]Universidade Estadual de Campinas, IFGW, Campinas, SP, Brazil

[21]Universidade Estadual de Feira de Santana, Feira de Santana, Brazil

[22]Universidade Federal do ABC, Santo André, SP, Brazil

[23]Universidade Federal do Paraná, Setor Palotina, Palotina, Brazil

[24]Universidade Federal do Rio de Janeiro, Instituto de Física, Rio de Janeiro, RJ, Brazil

[25]Universidade Federal do Rio de Janeiro (UFRJ), Observatório do Valongo, Rio de Janeiro, RJ, Brazil

[26]Universidade Federal Fluminense, EEIMVR, Volta Redonda, RJ, Brazil

[27]Universidad de Medellín, Medellín, Colombia

[28]Universidad Industrial de Santander, Bucaramanga, Colombia

[29]Charles University, Faculty of Mathematics and Physics, Institute of Particle and Nuclear Physics, Prague, Czech Republic

[30]Institute of Physics of the Czech Academy of Sciences, Prague, Czech Republic
[31]Palacky University, RCPTM, Olomouc, Czech Republic
[32]Institut de Physique Nucléaire d'Orsay (IPNO), Université Paris-Sud, Univ. Paris/Saclay, CNRS-IN2P3, Orsay, France
[33]Laboratoire de Physique Nucléaire et de Hautes Energies (LPNHE), Universités Paris 6 et Paris 7, CNRS-IN2P3, Paris, France
[34]Univ. Grenoble Alpes, CNRS, Grenoble Institute of Engineering Univ. Grenoble Alpes, LPSC-IN2P3, 38000 Grenoble, France
[35]Bergische Universität Wuppertal, Department of Physics, Wuppertal, Germany
[36]Karlsruhe Institute of Technology, Institute for Experimental Particle Physics (ETP), Karlsruhe, Germany
[37]Karlsruhe Institute of Technology, Institut für Kernphysik, Karlsruhe, Germany
[38]Karlsruhe Institute of Technology, Institut für Prozessdatenverarbeitung und Elektronik, Karlsruhe, Germany
[39]RWTH Aachen University, III. Physikalisches Institut A, Aachen, Germany
[40]Universität Hamburg, II. Institut für Theoretische Physik, Hamburg, Germany
[41]Universität Siegen, Fachbereich 7 Physik – Experimentelle Teilchenphysik, Siegen, Germany
[42]Gran Sasso Science Institute, L'Aquila, Italy
[43]INFN Laboratori Nazionali del Gran Sasso, Assergi (L'Aquila), Italy
[44]INFN, Sezione di Catania, Catania, Italy
[45]INFN, Sezione di Lecce, Lecce, Italy
[46]INFN, Sezione di Milano, Milano, Italy
[47]INFN, Sezione di Napoli, Napoli, Italy
[48]INFN, Sezione di Roma "Tor Vergata", Roma, Italy
[49]INFN, Sezione di Torino, Torino, Italy
[50]Osservatorio Astrofisico di Torino (INAF), Torino, Italy
[51]Politecnico di Milano, Dipartimento di Scienze e Tecnologie Aerospaziali , Milano, Italy
[52]Università del Salento, Dipartimento di Matematica e Fisica "E. De Giorgi", Lecce, Italy
[53]Università dell'Aquila, Dipartimento di Scienze Fisiche e Chimiche, L'Aquila, Italy
[54]Università di Catania, Dipartimento di Fisica e Astronomia, Catania, Italy
[55]Università di Milano, Dipartimento di Fisica, Milano, Italy
[56]Università di Napoli "Federico II", Dipartimento di Fisica "Ettore Pancini", Napoli, Italy
[57]Università di Roma "Tor Vergata", Dipartimento di Fisica, Roma, Italy
[58]Università Torino, Dipartimento di Fisica, Torino, Italy
[59]Benemérita Universidad Autónoma de Puebla, Puebla, México
[60]Centro de Investigación y de Estudios Avanzados del IPN (CINVESTAV), México, D.F., México
[61]Unidad Profesional Interdisciplinaria en Ingeniería y Tecnologías Avanzadas del Instituto Politécnico Nacional (UPIITA-IPN), México, D.F., México
[62]Universidad Autónoma de Chiapas, Tuxtla Gutiérrez, Chiapas, México
[63]Universidad Nacional Autónoma de México, México, D.F., México
[64]Institute of Nuclear Physics PAN, Krakow, Poland
[65]University of Łódź, Faculty of Astrophysics, Łódź, Poland
[66]University of Łódź, Faculty of High-Energy Astrophysics, Łódź, Poland

[67]Laboratório de Instrumentação e Física Experimental de Partículas – LIP and Instituto Superior Técnico – IST, Universidade de Lisboa – UL, Lisboa, Portugal

[68]"Horia Hulubei" National Institute for Physics and Nuclear Engineering, Bucharest-Magurele, Romania

[69]Institute of Space Science, Bucharest-Magurele, Romania

[70]University Politehnica of Bucharest, Bucharest, Romania

[71]Center for Astrophysics and Cosmology (CAC), University of Nova Gorica, Nova Gorica, Slovenia

[72]Experimental Particle Physics Department, J. Stefan Institute, Ljubljana, Slovenia

[73]Universidad de Granada and C.A.F.P.E., Granada, Spain

[74]Instituto Galego de Física de Altas Enerxías (I.G.F.A.E.), Universidad de Santiago de Compostela, Santiago de Compostela, Spain

[75]IMAPP, Radboud University Nijmegen, Nijmegen, The Netherlands

[76]KVI – Center for Advanced Radiation Technology, University of Groningen, Groningen, The Netherlands

[77]Nationaal Instituut voor Kernfysica en Hoge Energie Fysica (NIKHEF), Science Park, Amsterdam, The Netherlands

[78]Stichting Astronomisch Onderzoek in Nederland (ASTRON), Dwingeloo, The Netherlands

[79]Universiteit van Amsterdam, Faculty of Science, Amsterdam, The Netherlands

[80]Case Western Reserve University, Cleveland, OH, USA

[81]Colorado School of Mines, Golden, CO, USA

[82]Department of Physics and Astronomy, Lehman College, City University of New York, Bronx, NY, USA

[83]Louisiana State University, Baton Rouge, LA, USA

[84]Michigan Technological University, Houghton, MI, USA

[85]New York University, New York, NY, USA

[86]Pennsylvania State University, University Park, PA, USA

[87]University of Chicago, Enrico Fermi Institute, Chicago, IL, USA

[88]University of Delaware, Bartol Research Institute, Department of Physics and Astronomy, Newark, USA

[89]University of Nebraska, Lincoln, NE, USA

—

[1000]School of Physics and Astronomy, University of Leeds, Leeds, United Kingdom

[1001]Max-Planck-Institut für Radioastronomie, Bonn, Germany

[1002]Fermi National Accelerator Laboratory, USA

[1003]also at Universidade Federal de Alfenas, Poços de Caldas, Brazil

[1004]Colorado State University, Fort Collins, CO, USA

[1005]now at the Hakubi Center for Advanced Research and Graduate School of Science at Kyoto University

[1006]also at Karlsruhe Institute of Technology, Karlsruhe, Germany

[1007]also at University of Bucharest, Physics Department, Bucharest, Romania

Corresponding author: The Pierre Auger Collaboration (R. Engel), auger_spokespersons@fnal.gov

Key Points:

- Elves observed in Argentina, known for severe convective thunderstorms.
- UV fluorescence detector with a viewing footprint for elves of three million sq. km.
- Cameras with 10 MHz frame rate, revealing the internal EMP structure.
- Facility continuing year-round operation through at least 2025.

Abstract

Elves are a class of transient luminous events, with a radial extent typically greater than 250 km, that occur in the lower ionosphere above strong electrical storms. We report the observation of 1598 elves, from 2014 to 2016, recorded with unprecedented time resolution (100 ns) using the Fluorescence Detector (FD) of the Pierre Auger Cosmic Ray Observatory. The Auger Observatory is located in the Mendoza province of Argentina with a viewing footprint for elve observations of $3 \cdot 10^6$ km^2, reaching areas above the Pacific and Atlantic Oceans, as well as the Córdoba region, which is known for severe convective thunderstorms. Primarily designed for ultra-high energy cosmic-ray observations, the Auger FD turns out to be very sensitive to the UV emission in elves. The detector features modified Schmidt optics with large apertures resulting in a field of view that spans the horizon, and year-round operation on dark nights with low moonlight background, when the local weather is favorable. The measured light profiles of 18% of the elve events have more than one peak, compatible with intra-cloud activity. Within the three years sample, 72% of the elves correlate with the far-field radiation measurements of the World Wide Lightning Location Network (WWLLN). The Auger Observatory plans to continue operations until at least 2025, including elve observations and analysis. To the best of our knowledge, this observatory is the only facility on Earth that measures elves with year-round operation and full horizon coverage.

1 Introduction

In the 1990s, Inan et al. predicted quantitatively that ionospheric heating by electromagnetic pulses (EMP) originating from lightning strokes would create a transient flash of light expanding radially faster than the speed of light [*Inan et al.*, 1991, 1997]. The first finite-difference time-domain model effectively showed that the energy density of some very low frequency EMPs was sufficient to heat the plasma at the base of the E-layer of the nighttime ionosphere, and induce the fluorescence process of molecules [*Taranenko et al.*, 1993]. Since, numerous multidimensional simulations have used electromagnetic or "engineering" return stroke models [*Baba and Rakov*, 2007; *Rakov and Uman*, 1998] to create the EMP and predict the spatio-temporal structure and brightness of the light emission at the base of the ionosphere [*Cho and J. Rycroft*, 2001; *Marshall*, 2012; *Veronis et al.*, 1999].

The first observation of the "airglow enhancement", known to be a Transient Luminous Event (TLE), was captured in 1990 using video cameras with a 33 ms time resolution ($\Delta\tau$) aboard the Discovery Space Shuttle [*Boeck et al.*, 1992]. Five years later, in 1995, a multi-channel photometer ($\Delta\tau$ = 15 µs) and two CCDs ($\Delta\tau$ = 17 ms) made the first ground-based observation of Emissions of Light and Very low frequency perturbations due to Electromagnetic pulse Sources, or elve(s) [*Fukunishi et al.*, 1996]. The Imager of Sprites and Upper Atmospheric Lightning (ISUAL), launched aboard FORMOSAT-2 in 2004, was the first satellite instrument to make a global survey of elve occurrences [*Chern et al.*, 2003; *Mende et al.*, 2005]. Using a CCD imager ($\Delta\tau$ = 14 ms), a spectrophotometer ($\Delta\tau$ = 100 µs), and two array photometers ($\Delta\tau$ = 5 µs) consisting of one photomultiplier each, ISUAL concluded that the highest density of elves was over the ocean [*Chen et al.*, 2008]. In 2008, the Photometric Imager of Precipitated Electron Radiation (PIPER) ($\Delta\tau$ = 40 µs) detected the first elve "doublet", with two peaks in the photo-trace, during a summer field campaign [*Newsome and Inan*, 2010]. These doublets were first thought to originate from the short rise time of the current waveform in the return stroke process (Marshall, 2012); however, the wide time separation between the peaks was later confirmed experimentally to correlate with high altitude compact intra-cloud lightning discharges (CIDs) [*Marshall et al.*, 2015; *Lyu et al.*, 2015]. In 2017, elve "multiplets", with more than two peaks in the photo-trace, separated by much shorter time than previously observed, were anticipated to correlate with energetic in-cloud pulses (EIPs). EIPs were also believed to be responsible for the creation of particular terrestrial gamma ray flashes (TGFs) [*Liu et al.*, 2017]. These and other advances in detector sensitivity, including the facility described hereafter, and in lightning modeling suggest that multi-peaked elve measurements can be used to improve the understanding of the return stroke process in EIPs and CIDs, to study the link between elves and TGFs, and possibly, to provide insights into the initial breakdown (IB) processes [*Marshall et al.*, 2014; *da Silva and Pasko*, 2015]. Additionally, the study of single-peaked elves, known to be initiated by cloud-to-ground lightning, will help confirm the validity and limits of previously mentioned models at the most extreme lightning energies.

The Pierre Auger Observatory [*Aab et al.*, 2015] was designed to measure Ultra-High Energy Cosmic Rays (UHECR). As it turns out, the installed Fluorescence Detector (FD) [*Abraham et al.*, 2010; *Allekotte et al.*, 2008] has been observing elves since its debut in 2004 [*Mussa and Ciaccio*, 2012]. The elves are observed above strong lightning strokes that lie below the horizon. Located on four different sites, FD telescopes point in fixed directions. As the field of view (FoV) of the telescopes overlap, the 360° azimuthal coverage of the detector is spanned more than once. The same elve may be measured by multiple FD telescopes, each with an optical aperture of 2.2 m diameter and a time resolution ($\Delta\tau$ = 100 ns) unprecedented in the field of TLE observations. The combination enables detailed measurements of large numbers of single-peaked and multi-peaked elves.

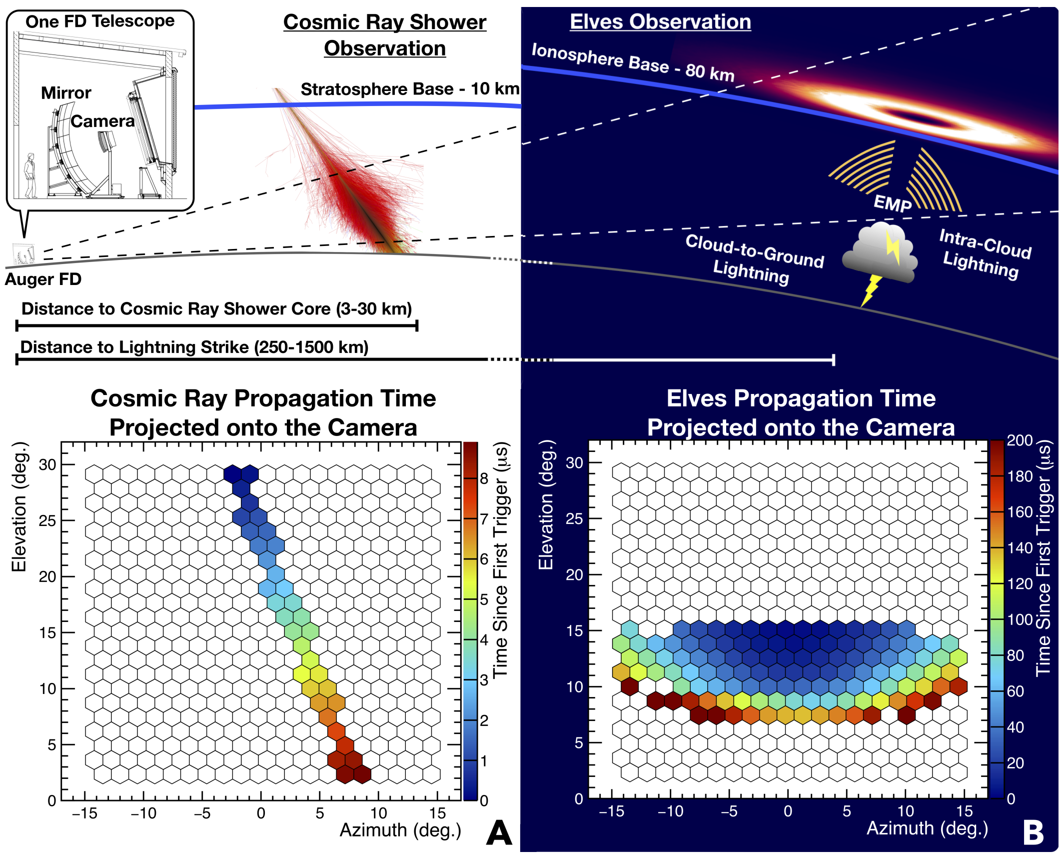

Figure 1. Top panel: a diagram of the FD telescope with its 3.6 m diameter mirror at the Pierre Auger Observatory [*Abraham et al.*, 2010] . The FD, optimized for the detection of cosmic rays up to 30 km, also turns out to be sensitive to elve signatures that are 1000 km away. The axes of lowest pixels have an elevation angle of 1.5° while the axes of highest pixels have elevation angles of 30°. Panel A: the time signature of a cosmic-ray shower propagating from top to bottom. Panel B: the first 200 μs of the propagation of an elve across an FD telescope camera field of view, showing the one side of the elves expanding towards the detector.

When an UHECR strikes the atmosphere, its kinetic energy is converted into an air shower of relativistic secondary particles, mostly electrons, positrons and muons. These secondary particles collide inelastically with molecules in the troposphere, exciting the local nitrogen. The UV emission, also known as fluorescence, occurs from the fast de-excitation of N_2 molecules, previously excited by low-energy ionization electrons left after the passage of the electromagnetic cascade in the troposphere [*Arqueros et al.*, 2008; *Rosado et al.*, 2014]. The optics of the FD telescopes are optimized to capture the faint UV light arriving from the UHECR air shower development (Figure 1, panel A). As for elves, the EMPs caused by the return strokes accelerate charged particles, primarily electrons, at the base of the ionosphere. The collisions between the particles and nitrogen molecule produce UV fluorescence light that is also observed by the FD (Figure 1, panel B). Due to the fast radiative process of nitrogen in the UV (40 ns) [*Valk et al.*, 2010], an elve measurement with a 100 ns time resolution is almost equivalent to a direct observation of the EMP. UHECR air showers are visible between about 3 and 30 km from a given FD site, depending on their energy. In contrast, the elves are much brighter due to the energy scale of lightning being much higher. The Auger Observatory has observed elves as far away as 1500 km.

Using the fact that 95% of the observed elves are within 1000 km from the Auger Observatory, which is beyond the distance where the axes of the lower pixels intercept a 92 km ionosphere, we can estimate the observational footprint of the Auger FD for elves to be $3 \cdot 10^6\,\text{km}^2$. This footprint covers portions of the Pacific Ocean, the Atlantic Ocean, Chile, the Andes mountain range and Northern Argentina. The latter includes the Córdoba region, known for some of the most energetic and destructive convective thunderstorm systems in the world [*Rasmussen et al.*, 2014] and the highest lightning flash rate in some of the tallest thunderstorms [*Zipser et al.*, 2006]. The measurements of elves by the Auger Observatory, including many from this region of special interest, are expected to further the understanding of mechanisms that govern the production of the most intense lightning and to improve current models. The Auger Observatory will continue year-round operations, including observations of elves during dark night periods, until at least 2025.

In 2014, the FD readout and triggering algorithms were updated to better identify elve signatures and to record up to 300 µs of signal for each pixel of the camera. Hence, we report on 1598 reconstructed, verified elves that were observed in the three-year acquisition period, from 2014 to 2016. Using the unique capabilities of the FD, we sorted the data into two categories: 1310 single-peaked and 288 multi-peaked elves. More extensive analysis of this dataset will be published in future articles.

Table 1. Parameters of the Fluorescence Detector

Item	Value	Note
Number of FD sites	4	located on footprint outskirts
Number of telescopes per site	6	180° azimuthal field of view
Telescope optical aperture	2.2 m	extended diameter with corrector ring
Field of view of one telescope	$30° \times 30°$	azimuth×elevation
Number of pixels per telescope	440	hexagonally shaped
Field of view of one pixel	$1.5° \times 1.5°$	
Optical filter	Schott MUG-6	bandwidth: 300 - 420 nm, >680 nm
Photomultiplier tube quantum efficiency	30%	340 - 420 nm (0% above 700 nm)
Time bin length	100 ns	typically binned to 2 μs for long traces
Readout duration	100-300 μs	including a 28 μs pedestal
Absolute photometric calibration	±7%	

2 The Pierre Auger Observatory

The Auger Observatory measures the properties of the most energetic particles known to exist in the Universe and aims to discover their sources. The energy of a single "cosmic ray" particle can reach 10^{20} eV, an energy scale well beyond the reach of man-made accelerators. Ground-based cosmic-ray observatories are designed to detect secondary particles that are created when a high energy subatomic particle, from galactic or extragalactic origins, interacts with the atmosphere of the Earth. Cosmic rays collide with molecules in the troposphere or the lower stratosphere and create extended air showers, which the Auger Observatory measures using a surface array of 1600 water-Cherenkov detectors (SD), spanning 3000 km^2, and a set of fluorescence detectors (FD) [*Abraham et al.*, 2010; *Allekotte et al.*, 2008].

We focus here on parameters of the FD (Table 1) that are important for the observation of elves. The FD telescopes (Figure 2, panel A) point in fixed directions, ≈17° above the horizontal. The pointing directions, FoV, mirrors, UV optical filters, and photomultiplier tube cameras are optimized to measure the faint 300-400 nm light arriving from UHECR air showers through the troposphere. The quantum efficiency of the photomultiplier tubes is null above 700 nm and the UV filter is opaque below 680 nm, limiting the detection of red and infra-red light for all TLEs. Typical UHECR signals at the FD aperture are tens to thousands of photons/m^2/100 ns, and typical viewing distances range from 3 to 30 km. In contrast, more than 95% of the observed elves are 250-1000 km away, where the FoV of a telescope crosses the ionosphere and direct light from lightning is blocked by the limb of the Earth. In the signal observed at the FD, the higher intrinsic brightness of elves relative to the UHECRs compensates for the further distance to the elves. The tallest peak in the Andes mountain range may partly obstruct the last three rows of the telescopes pointing east, limiting the reconstruction of elve-inducing lightning beyond 1000 km distances. The Auger FD operates on locally clear nights with low background from moonlight, accumulating about 1200 hours of FD on-time over 12 months, equivalent to a 15% duty cycle. A suite of lasers, lidars, IR cloud cameras measures the optical clarity of the atmosphere over the observatory [*Aab et al.*, 2013a].

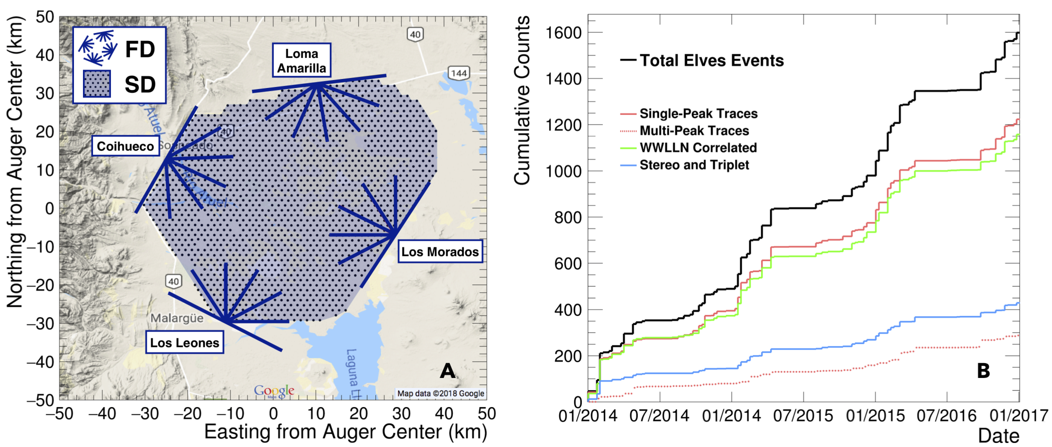

Figure 2. Panel A: the physical footprint of the Pierre Auger Cosmic-Ray Observatory is defined by the location of water-Cherenkov stations making up the Surface Detector (SD). The Fluorescence Detector (FD), used for the observation of elves, has a total of 24 telescopes positioned at four different sites on the outskirts of the SD. Six adjacent telescopes have a 180° field of view. Panel B: the cumulative elve data acquired by the Auger FD reached 1598 counts in the 2014-2016 acquisition period. The count of elves with one peak in the photo-traces is contrasted to the count of multi-peaked elves. The number of Auger elves that are correlated to a WWLLN event within 5 ms is displayed in green.

The FD telescopes are located at four sites. Six telescopes at each site are arranged for a total FoV of 180° (azimuth) × 30° (elevation). Due to the geometrical orientation of the FD sites, the physical aperture of the detector for the observation of elves is broken in three overlap regions: 8% seen by one site, 74% seen by two sites, and 18% seen by three sites. Detection probabilities due to variability in coverage are discussed in Section 5.

The data readout of the Auger FD includes three trigger levels to select events of interest. The analog signals for each pixel are digitized every 100 ns and pass the first level trigger (FLT) if the analog-to-digital conversion (ADC) threshold requirement is satisfied. The second level trigger (SLT) is a pattern recognition designed to select UHECR signals; it requires at least four adjacent pixels passing the FLT. To form an event of interest and to be saved to disk, the traces have to pass the more complex third level trigger (TLT).

As part of the active interdisciplinary program pursued by the Auger Collaboration, we developed a TLT for lightning noise. Due to the time structure of the photo-traces and the number of triggered pixels, these events are primarily detected by this lightning TLT. Then, the events are searched for a radially expanding light front. Once the first triggered pixel is identified, pulse start times of the adjacent triggered pixels are required to have a monotonic growth. The trigger tolerates 20% of pixels that do not satisfy this cut. The algorithm requests at least three adjoining pixels to satisfy the described cut, on both sides of the first signal (only one side is required if the first pixel is close to the edge of a camera) and at least another three neighboring pixels above and below it.

3 Collected Data and Reconstruction of Lightning Location

The Pierre Auger Observatory started taking data in 2004. The fourth FD site, at Loma Amarilla, started operations in 2007. The first elve was observed in 2005, and two more events, which occurred in 2007, were discovered in a search for exotic events performed in 2009. A thorough search for elves in randomly saved events with loose trigger requirements, harvested in the period from 2007 to 2011, was exploited to design a modified TLT algorithm. The search yielded 58 more candidates [*Aab et al.*, 2013b]. In 2013, the observatory started acquiring elve candidates with the standard trace length (100 μs) and in 2014, we improved the TLT to acquire up to 300 μs of signal. In what follows, we present the data acquired during the 2014-2016 time period, for which we can now provide a more accurate reconstructed location and time. A seasonal dependence is present in the cumulative count of elves (Figure 2, panel B). The three elongated flat regions correspond to the southern winter, June through August, when 43 elves were recorded over the course of three years. In contrast, we captured 711 elves over three summers. The discrete steps of the cumulative plot matched the nightly acquisition periods of the FD, as defined by the lunar cycle.

The first 28 μs of the recorded traces occurred before the first photons from the emission region hit the detector and were used to calculate the baselines for each pixel; consequently, the true length of traces was 272 μs. Because the FoV of individual FD sites overlap, we categorized elve candidates as mono (detected at one site), stereo (detected at two sites), or triplet (detected at three sites). We required that the same event was observed at all sites within 200 μs. The raw dataset consists of 2311 elve candidates, including 1864 mono, 396 stereo, and 51 triplet. To further increase the purity of the data sample, we verified that each candidate portrays the expected time structure and signal amplitude, and then we performed a geometric reconstruction.

With a 100 ns resolution, the FD distinguishes variations in the light emission caused by the internal structure of the EMP. Marshall et al., and numerous others, show quantitatively through analytics and numerics that the EMP created by cloud-to-ground (CG) lightning will structurally differ from an intra-cloud (IC) discharge [*Marshall*, 2012]. The ground is treated as a perfect conductor, which is a good approximation for very low frequency radiation of about 10 kHz. The physical process of the return stroke is trivialized to a current pulse traveling at a fraction of the speed of light along a wire [*Rakov and Uman*, 1998], and modeled as a Hertzian dipole, which is analytically solved using the method of images. We expect CG flashes, which are in contact with the ground, to radiate one large pulse directly towards the ionosphere. However, the IC flashes, not touching the conductor, would have the upper hemisphere of the dipole field radiate towards the ionosphere and the lower hemisphere of the dipole field radiate towards the ground. The downward propagating pulse bounces off the ground and travels behind the upward propagating pulse, reaching the ionosphere as a secondary pulse with a time delay related to the height of the lightning stroke. Due to the maximum height of clouds reaching about 17 km, we expect the presence of secondary pulses in the FD's photo-traces, within 150 μs from the primary pulses, to be a hint of IC lightning activity. More complex physics may also be a cause of such structures. Selecting specific time decay constants of the current profile in the return stroke leads to substructure within the primary and secondary pulses [*Liu et al.*, 2017]. Initial breakdown (IB) pulses have been recorded within tens of microseconds from one another and could create multiple elves [*da Silva and Pasko*, 2015]. Since multiple return strokes occur at the millisecond time scale and radiate significantly less energy, we do not interpret them as a cause of the internal structure observed in the Auger elve events. Finally, elves are distinctly different from other TLEs in the same vicinity to the ionosphere (sprites and halos). Sprites, mainly caused by the strong quasi-static fields of thunderstorms, would propagate vertically above the cloud and would not fit the geometry observed in the FD. On the other hand, sprite halos, also disk-shaped and radially expanding, typically expand between 50 and 100 km and occur milliseconds after the stroke, while elves happen ≈270 μs after the stroke [*Miyasato et al.*, 2003]. Compared to halos, almost all elves have a distinct hole in the center due to the shape of the dipole radiation and they expand to radii greater than 200 km.

From the intrinsic time scale of the expanding elves, their varying locations and the projected geometry at hand, we expected the amplitude, mean and width of the observed traces to vary significantly depending on the pixel. When looking at pixels away from the first triggered pixel, the traces became wider and asymmetric. Also, the start time and amplitude of the pulses increased monotonically. A verification process, further described below, assessed whether candidates satisfied the expected trends: 1727 of the candidate events were approved as elves, though not yet reconstructed.

In the verification process, we identified 1403 single-peaked elves, suggesting that a cloud-to-ground (CG) lightning radiated the EMP. In panel A of Figure 3, we show traces of a typical single-peaked elve event binned to 2 μs to reduce the clutter in the plot. By recording the time of the peak maximum, we created the time propagation plot in panel B of Figure 1. We also integrated 10 μs of the photo-traces at relevant times to create snapshots of the signal in the telescope camera (Figure 3, panel B). The arc-shaped signal correlated to a signal propagating up the camera, towards lower elevation angles. The cameras triggered on the outer most edge of the elve (disk shaped with ≈250 km radius), closest to the observatory, and later acquired the signal above the lightning strike. The FD only recorded the half of the flash propagating towards the Auger Observatory. Patterns observed across all elve events are well featured in this example:

- the first pulse detected indicates the location of the shortest light propagation path to the lightning strike;
- the signal propagates down the rows with a rise in total photon count and pulse start time, until the hole above the lightning is reached;

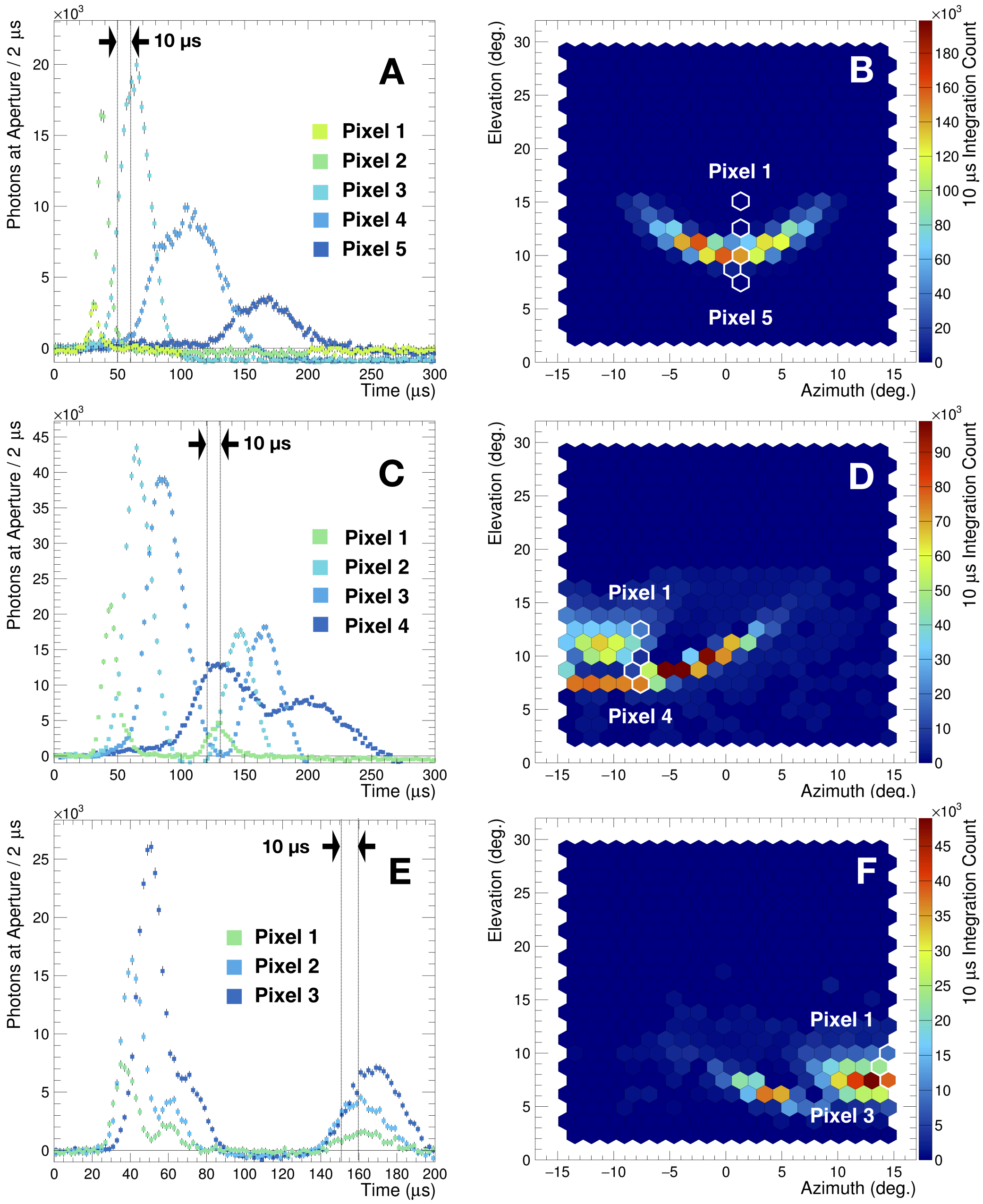

Figure 3. Panel A: Some 300 µs-long traces of typical single-peaked elve observed in the FD at Los Leones, on February 2^{nd}, 2014 at 05:12:22. Panel B: we selected 10 µs of signal captured by the camera to show the arc-shape of the elve. Panel C and D: selected traces and a 10 µs snapshot of a double-peaked event seen in Coihueco, on January 17^{th}, 2016 at 04:52:31 UTC. Panel E and F: 200 µs-long traces and a 10 µs snapshot of a multi-peaked event seen in Los Leones, on March 4^{th}, 2016 at 05:32:39 UTC.

- the lack of emission due to the dipole radiation pattern above the lightning strike is noticeable with the 300 µs acquisition time used for the dataset presented here;

- the amplitudes of the traces are strongly affected by the amount of atmosphere between the emission and the mirror;
- and the increased asymmetry of the pulses down the camera rows are a result of a wider observation area for pixels pointing at low elevation angles.

In addition to the single-peaked elves, we recognized 324 multi-peaked elves (18% of our dataset), with trends in the traces that are similar to the single-peaked elves. Typical multi-peaked events have two distinct maxima; however, some events may have more than two distinguishable peaks. In panels C and D of Figure 3, we present a typical double elve as observed by the Auger FD. In the first selected pixel (Pixel 1, in green), two peaks are separated by ≈90 μs. To illustrate the FD resolution, we also display traces of an event with three clearly distinguishable peaks (Figure 3, panels E and F). This structure is observed independently at two FD sites separated by 40 km, Coihueco and Loma Amarilla. In the first 100 μs, the two telescopes recorded two peaks separated by ≈20 μs in three selected pixels on the right of the camera. These two peaks may originate from IB discharges or more complex current profiles, as described previously. In the following 100 μs, we are able to fit the third peak with the standard deviation of the first two combined. We interpret the third peak to be the bounces of the secondary pulses on the ground, distorted by the reflection and their projection on the ionosphere. In the case of an inclined dipole, we expect discrepancies in pulse amplitudes, often the case in IC discharge [*Marshall et al.*, 2015].

We also performed a reconstruction of the location and time of the elve-inducing lightning. We first fitted ADC trace for each pixel to an asymmetric Gaussian parametrized with the mean time, the signal amplitude and the skewness, which related the left and right standard deviations: $T_{\mathrm{peak},i}$, $A_{\mathrm{peak},i}$, $\sigma_{\mathrm{left},i}$, and $\sigma_{\mathrm{right},i} = \sigma_{\mathrm{left},i} \cdot (1 + \delta)$, where i is the index of the pixel. When dealing with multi-peaked elves, we selected the set of peaks ordered in time with the highest amplitude peak in the first triggered trace. Each pulse had to pass four quality criteria to be part of the reconstruction of the lighting location and time:

- $A_{\mathrm{peak},i}$ greater than 300 ADC counts to select triggered pixels with sufficient signal,
- a relative error on $A_{\mathrm{peak},i}$ below 15% to disregard any traces with distorted profiles,
- $\sigma_{\mathrm{left},i}(T)$ greater than 3 μs to encompass the width of the trace in the first triggered pixel and all subsequent signals,

Table 2. Elves counts through different stages of the analysis. Each row is a subset of the one above.

Stage	Mono	Stereo	Triplet	Total	Note
Triggered	1864	396	51	2311	independent of FD on-time
Verified	1287	390	50	1727	features typical elve profile
Confirmed	1169	379	50	1598	reconstructed at at least one site
WWLLN Correlated	836	284	38	1158	5 ms coincidence

- a relative error on $\sigma_{\mathrm{left},i}(T)$ below 25% to enforce the quality of the fit.

The parameters from the first fit were inputs to the second fit of the reconstruction, where we used a χ^2-minimization to obtain the time, latitude, longitude, and height (H_S) of the lightning strike, and the height of the emission region at the base of the ionosphere (H_E):

$$\chi^2 = \Sigma_{i=1}^{N_\mathrm{pix}} (T_{\mathrm{peak},i} - T_{\mathrm{estimate},i})^2 / \sigma_i^2(T)$$

where $T_{\mathrm{estimate},i} = T_0 + \Delta T(\mathrm{Lat}, \mathrm{Lon}, H_\mathrm{E}, H_\mathrm{S})$ was the estimated time at which light reached the detector after the propagation time, ΔT, when added to the time of the lightning strike, T_0. We minimized the χ^2 by incrementally varying the position and time of the lightning, as well as the height of the ionosphere. The error on $T_{\mathrm{peak},i}$ came from the fit of the pixel trace. The model assumed that the EMP generated by the return stroke interacted in an infinitesimal layer at an atmospheric altitude H_E. The nitrogen fluorescence happens at negligible time scales (≈40 ns [*Valk et al.*, 2010]) with respect to the total light propagation time from the strike to the detector, and with respect to the integration time of the camera.

In this paper, we present results with two constrained variables to reduce the complexity of the reconstruction. The fit allows Lat, Lon and T_0 to vary while fixing H_E at 92 km and H_S at the ground, even for multi-peaked elves. We base our guess of the ionosphere height on our timing correlation with WWLLN (presented in the next section), a few kilometers higher in altitude than observations made in South-Western Europe [*van der Velde and Montanyà*, 2016]. The South Atlantic Anomaly may be a factor affecting the altitude of the ionosphere base.

Ultimately, we may have observed an event at more than one FD site but reconstructed it solely once. Hence, we define a *confirmed* elve event as one that passed the verification stage and that was reconstructed at least once. In this three-year dataset, we found 1598 confirmed elve flashes. In addition, the coverage of WWLLN in Argentina is such that three antennas are within the observational footprint for elves of the Auger FD [*Jacobson et al.*, 2006; *Hutchins et al.*, 2012a]. Our correlation with the network was 72%: 1158 Auger elves correlated within 5 ms of a WWLLN reconstructed lightning strike. A finer time correlation study will be presented in the next section. We summarize all event counts in Table 2.

4 Time Correlation, Energy Distribution and Spatial Resolution

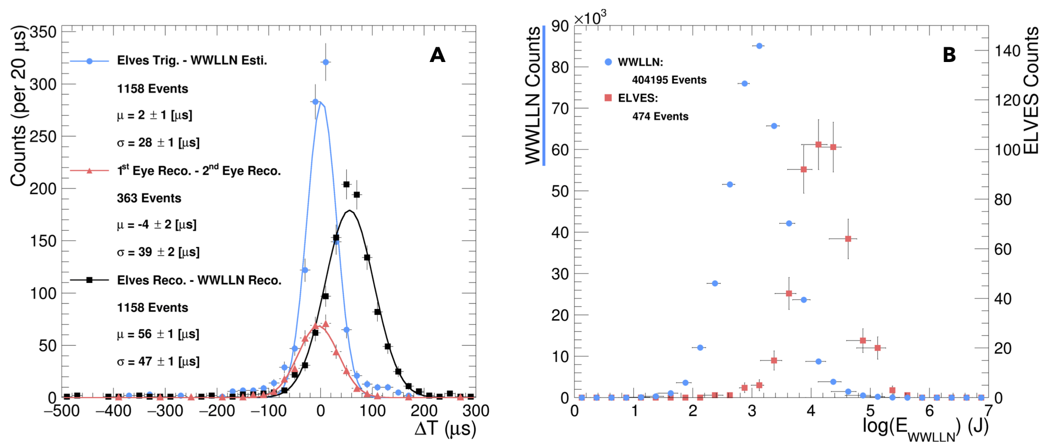

Figure 4. Panel A: the timing correlation between the reconstructed lighting strike of WWLLN, added to the shortest propagation time from the strike location to the Auger FD, and triggered time stamp in the FD, shown in red. The difference between two independent reconstructions of the same elve observed at two FD sites is shown in blue. Panel B: comparison between the distribution of lightning energy for all WWLLN events measured in the FoV of the active FD and those WWLLN events correlated to elves measured by Auger, from 2014 through 2016.

To refine the timing correlation with WWLLN, we estimate the shortest propagation time of light from the lightning strike reconstructed by WWLLN to the ionosphere, and finally to the FD detector. For most elves, we suggest that the point on the ionosphere, halfway between the lightning strike and the FD, is where the first light emission would occur. Any elve not large enough to reach that halfway point has an underestimated time of the lightning strike. If the height of the ionosphere is not well chosen, then all time estimates are also miscalculated. After adding the calculated propagation time to the WWLLN reconstructed strike time, assumed to be at the ground, we compare the result to the Auger FD trigger time (Figure 4, panel A, blue curve). The mean of the distribution is sensitive to the height of the infinitesimal ionospheric layer, where the emission is assumed to originate. If the ionosphere height is overestimated, light traveled a longer distance to reach the detector, and we overestimate the time at which the first photons reached the FD. A 92 km ionosphere base has almost no offset on the position of the mean, $\mu_{\mathrm{WWLLN}} = 2 \pm 1$ μs, while an 85 km height wrongly overestimates our trigger time by 20 ± 1 μs and a 100 km height underestimates it by 19 ± 1 μs. The WWLLN resolution in the Auger FoV drives the distribution width of 28 μs (≈8 km).

The reconstruction of elves provides an estimate of the lightning strike time based on the fitted location as measured at individual FD sites. We detailed this process in section 3. Comparing the results obtained at any two FD sites observing the same event, using 363 stereo and triplet events with all triggered sites reconstructed, yields an estimate of our reconstruction timing resolution (Figure 4, panel A, red curve). The 39 μs RMS indicates an FD mono resolution ($\sigma_{\mathrm{mono}} = \sigma_{\mathrm{stereo}}/\sqrt{2}$) of 28 μs (≈8 km). Hence, at first glance, our reconstruction is doing as well as the reconstruction of WWLLN at timing the lightning strike. Finally, we compare directly the Auger reconstruction and the WWLLN reconstruction (Figure 4, panel A, black curve). The standard deviation of the black curve is more than the Auger mono contribution and the WWLLN contribution added in quadrature, hence there is 5-10 μs of unknown systematics. With the current status of the reconstruction, we are able to almost match WWLLN in locating the lightning strikes, but we slightly overestimate the time at which the events happened. Both the WWLLN and the Auger reconstructions use signal traces as fundamental inputs. We do not know what part of the trace was used as the start time in the WWLLN reconstruction, which could contribute significantly to the offset observed in the black curve. Possible sources of error to explore are the differentiation between IC and CG sources in the WWLLN dataset, as well as in the elve dataset. Two additional parameters in the Auger reconstruction will be released for multi-peaked events to improve the timing resolution. In addition, elves are created from an EMP with a wider frequency band and a greater energy density than the EMP observed by WWLLN, hence we expect our photo-traces to differ from the direct observation of that network.

By applying a cut on the distance from the Auger Observatory on both the Auger elves and the WWLLN lightning strike (250 to 1000 km still selecting >95% of observed elves) and requiring all FD sites to be active (in data taking mode), we compare the energy of lightning which created elves to that of all lightning observed by WWLLN within this time and footprint (Figure 4, panel B). This distance cut is chosen to optimize the comparison between events of both datasets happening within the FoV of the Auger FD. WWLLN records the far-field radiated electromagnetic energy in the 6 to 18 kHz frequency band. The peak radiated energy is known to be in the 10 to 15 kHz range. The 474 confirmed elve events satisfying the above correlation requirements are correlated to WWLLN events at the high end of the energy spectrum. We omitted elves with more than one WWLLN event correlated within the 5 ms coincidence. Adding those events to the analysis uniformly increases the counts in the last four bins. To obtain the median energy of both datasets, we calculate the mean of the log-normal distributions to obtain 16 ± 2 kJ for the matched elves and 1.3 ± 0.1 kJ for all lightning. Using an empirical equation for peak current [*Hutchins et al.*, 2012b],

$$I_0 = (E_{\mathrm{WWLLN}}/(1.3 \cdot 10^{-3} \cdot 1676))^{0.6173}, \quad (1)$$

where E_{WWLLN} is the recorded far-field radiation energy in Joule, the calculated median energy for the 404195 selected WWLLN lightning strikes converts to a median peak current of 51 ± 3 kA. Equation 1 was obtained on low- to mid-energy lightning strikes. Because this range does not have a strong overlap with the 474 strikes matched to the Auger elve data, we do not provide a peak current for these strikes.

To illustrate the spatial resolution of the reconstructed lightning location obtained from elves, we transform from geodetic coordinates to a local Auger coordinate system. This transformation provides the reconstructed distance and azimuth of the lightning. In Figure 5, panels A and B, we present the difference between the reconstructed lightning locations of WWLLN and Auger, with respect to the location of the Auger FD. For comparison, we also provide the reconstructed lightning locations by the Auger Observatory for elves observed in stereo (Figure 5, panels C and D). For all the plots, the analysis requires more than 10 events in every 50 km bin for the calculation of a mean and RMS. The lighter color indicates the RMS in each bin, while the darker color portrays the statistical error on the mean. The uncertainties of both the WWLLN and Auger reconstruction contribute to the error of the blue plots. The current reconstruction of elves systematically overestimates the distance of the lightning strike by 15 km. This consistent offset

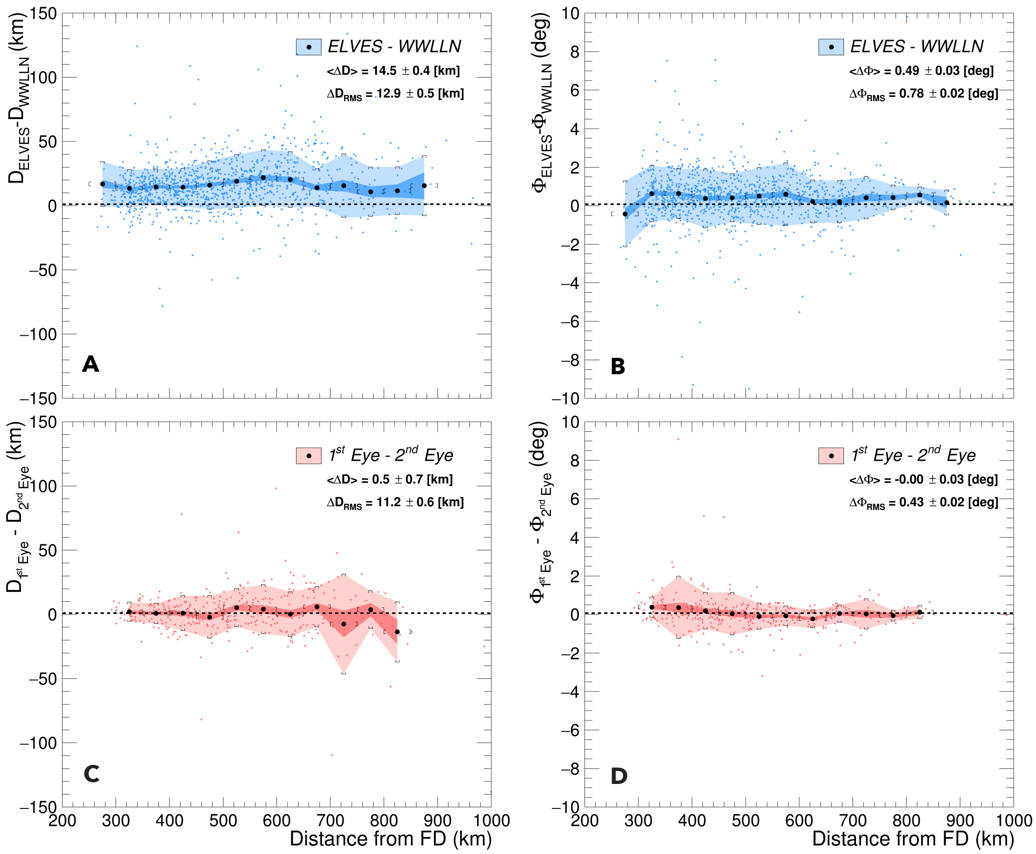

Figure 5. We present an assessment of the Auger reconstruction quality performed by converting all geodetic locations to a distance, D, and an azimuth, Φ, with respect to the observing FD site. The distance is the lightning strike distance from the triggered FD site, while the angle is the azimuth due east. Panel A and B: we compare the lightning strike location reconstructed by WWLLN to the location reconstructed from the observation of the elve. Panel C and D: we test the position resolution between two Auger reconstructions of a stereo or triplet observation.

as a function of distance from the Auger Observatory is compatible with the timing observed in Figure 4, hinting at a discrepancy between signal start times of Auger elves and WWLLN far-field radiation measurements. The combined RMS of the distance and azimuth difference plots also agrees with the timing resolution.

5 Lightning Location Maps

To disentangle dense elve regions from high observation probability regions, we display the reconstructed location of the elve-inducing lightning in four Mercator projected, high resolution maps (Figure 6). More than 90% of the elves detected by the Auger Ob-

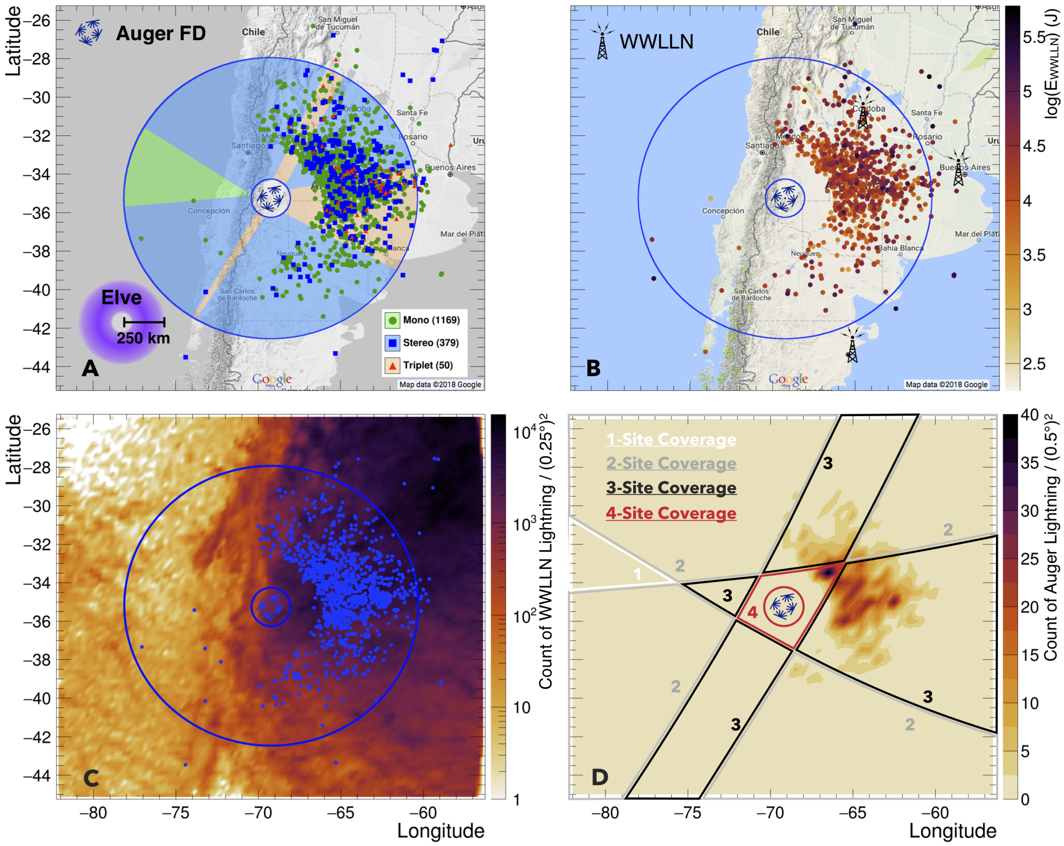

Figure 6. These maps denote the location of the reconstructed lightning strikes causing elves seen by the observatory, in geodetic coordinates. The large and small circles outline the lower and upper boundaries of the pixel array when projected to the base of the ionosphere, approximately with 860 km and 110 km radius, respectively. Panel A: the reconstructed lightning strike location from Auger elves and the number of FD sites contributing to each observation. The overlap of the FoV of each FD sites is shown in the shaded regions. Panel B: the WWLLN events correlated with our elve dataset against a log-color scale representing their energy in Joule. Panel C: a density map of WWLLN events with an overlay of elve-inducing lightning in coincidence. Panel D: the 1-site, 2-site, 3-site and 4-site coverage regions as an overlay on a density map of reconstructed locations of lightning strikes obtained from Auger elves.

servatory are to the east of the detector center (lat. = −35.25°, lon. = −69.25°). In contrast, we confirm only six events to the west of the Andes mountain chain. Two blue circles define the FD FoV projected onto a plane at 92 km altitude: the inner circle coincides with the upper edge of the pixels at 30° elevation from the ground, while the outer circle bounds the lower edge of the pixels at 1.5° elevation. These inner and outer contours are at 110 km and 860 km from the center of the Auger Observatory, respectively. Multiple

FD sites observing in the same region have a higher chance of an elve observation. We aim at disentangling our high detection probability in the north-east from the high occurrence of elves in that region.

Each data point in the maps is the location of the lightning strike reconstructed from an elve. The inhomogeneous strike density, as a function of distance from the center of the Auger Observatory, reveals unavoidable cutoffs for data acquisition in the observational footprint of the FD. When too close to the horizon, the light from the top of thunderstorm systems may reach the pixel array before the light emission from the ionosphere. The discarded lightning events induce a natural inner cutoff at $\approx$230 km.

We color the overlap regions of the detector FoV in green for mono, blue for stereo, and orange for triplet (Figure 6, panel A). As an overlay, we plot the location of the center of the elve (ie. the reconstructed lightning location) based on their observation duplicity. In the mono region, the FD recorded only one event despite the 1172 events observed only by one site in the rest of the FoV. Because the size of an elve, as defined by its UV emission region, spans a few hundred kilometers, we reconstructed 17 of the 50 triplet events outside a triplet overlap region. The proportionality of triplet events to mono and stereo events indicates a detection inefficiency induced by factors such as the trigger algorithms, the detector on-times, the reconstruction and other phenomenological effects such as clouds between the light emission and an FD site.

From the energy map of WWLLN events matched in time to Auger elves, we observe that the FD tends to trigger on higher energy events when the lightning location is outside the physical, projected aperture (Figure 6, panel B). At closer distances, the FoV overlap located east of the Auger Observatory increases the observation probability, and the light from the emission region travels through less atmosphere to reach the telescopes. Hence, the Auger FD triggers on numerous, dimmer events at near distances.

By cross-checking the on-time of the Auger FD with the WWLLN dataset, we created a density map of WWLLN lightning events displayed on a log scale with quarter geodetic degree bin size (Figure 6, panel C). From this heat map of WWLLN events acquired from 2014 to 2016, uncorrected for relative detection inefficiencies [*Hutchins et al.*, 2012a], we confirm the high density of lightning strikes present in the north-east of Argentina. The low density of lightning strikes over the ocean coincides with the low elve count observed by the Auger Observatory, consistent with the lightning climatology study of Virts et al. [*Virts et al.*, 2013]. In this map, we do not require an energy value from WWLLN as a selection for the elve events, but only a 5 ms timing coincidence.

To confirm the anisotropic elve distribution, we investigate the increased probability of observation in the surrounding overlap regions. Assuming a hypothetical flat elve at 92 km altitude, with an averaged radius of 250 km and an equal detection probability at all FD sites, we calculate the percentage of that elve in the FoV of each sites. The value for the elve radius is representative of the Auger dataset, it is much larger than what was previously reported by the PIPER experiment [*Blaes et al.*, 2014]. If at least 15% of the elve is in the FoV of an FD site, then we flag the center of that elve as a geodetic location with elve-inducing lightning, detectable by the Auger Observatory. From the number of FD sites which can detect at least 15% of the same elve, we infer coverage regions which differed from the overlap regions mentioned previously (Figure 6, panel D): 1-site, 2-site, 3-site and 4-site coverage. If lightning strikes in a 3-site coverage region, three FD sites will have at least 15% of the hypothetical elve in their FoV. This map of expected coverage configurations indicates the presence of a 4-site coverage region. If a 500 km diameter elve is centered around a geodetic locations in that 4-site coverage region, it covers two different triplet overlap regions. This map also suggests an expanded region for possible triplet observations, where the probability to make an observation in that 3-site region ($P = 1 - (1 - \epsilon)^3$, with ϵ representing the detection probability for one site) is greater than the probability of an observation in a 2-site region ($P = 1 - (1 - \epsilon)^2$). A superposition of the coverage with a heat map of the Auger reconstructed lightning location data explains the hot spot in the 4-site region ($P = 1-(1-\epsilon)^4$), at geodetic coordinates: (−33.5°,−66.5°).

We obtain an estimate for the probability from the lack of triplet observation in a 3-site coverage region, where most of the events occurred in this three year dataset. The ratio of mono to stereo counts, mono to triplet counts, or stereo to triplet counts are correlated, through basic probability theory, to an estimate of the observation probability for a single site of 35 ± 8%. Consequently, we calculate the probability to detect an elve by using the simple formulas mentioned previously, to be 82 ± 9% for an elve-inducing lightning in a 4-site coverage region (73 ± 10% in a 3-site region); however, this detection inefficiency leads to a probability of making a quadruplet observation (ϵ^4) closer to one in a hundred. With another few years of data, we anticipate the detection of an elve with all FD sites. Multiple-site observations also become a useful tool to understand the atmospheric attenuation and confirm the total amount of photons emitted at the base of the ionosphere. With the analysis described here, we will track the changes in our efficiencies after each improvement of the trigger algorithm. Ultimately, we will be able to obtain a number for the minimum lightning energy needed to create elves in our field of view.

6 Summary

After adding a new trigger channel to target a class of atmospheric TLEs known as elves, the Pierre Auger Observatory has recorded almost 1600 of these events over the three-year period from 2014 to 2016. This cosmic-ray observatory, located in the Mendoza province of Argentina, includes 24 fixed-direction UV-fluorescence photometric telescopes distributed over four different sites. These telescopes operate every night when the weather is reasonably clear and the moonlight is sufficiently low. The total field of view of the FD spans in azimuth the entire horizon and 92% of it is covered by two FD sites. Several hundred photomultiplier pixels, digitized at 10 MHz, participate in a typical elve measurement. The dataset reported here demonstrates that the observatory acceptance for elves extends over $3 \cdot 10^6$ km^2.

We developed an algorithm to reconstruct the latitude and longitude of the lightning from the measured light-time distributions of the recorded elves. A list of the coordinates, and UTC times of 1598 elves are available with this paper, on the website of the journal. When the height of the UV emission is constrained to 92 km above sea level, the current state of the resolution analysis shows that we agree with a WWLLN estimate of the FD trigger time. This analysis also shows that we slightly overestimate the distance and time of our reconstructed events. 72% of the observed elves correlate with independent radio-frequency measurements of lightning by WWLLN. For a quality subset of these correlated events (474), the lightning energy as measured by WWLLN had a median of 16 kJ, while the median energy of all lightning measured by WWLLN that occurred inside the elve footprint while the telescopes were taking data, was 1.3 kJ. Using this particular lightning dataset and lightning energies, the turn-on threshold for elve detection by the Auger Observatory is about an order of magnitude higher than the turn-on threshold for lightning detection by WWLLN.

The observed elve locations exhibited seasonal and geographical patterns: 44% of the elves observed occurred during the southern-summer months and just 2.5% occurred during winter months. Nearly all of the observed elves appeared east of the Andes and just two were observed and reconstructed over the Pacific Ocean, confirming a study by Virts et al. From the multiplicity of peaks in the traces, we conclude that 18% of our dataset was related IC lightning activity (at least two peaks in the photo-trace) while the rest shows simpler structure.

The Pierre Auger Observatory is scheduled to operate until at least 2025. In 2017, we implemented a deeper readout-window of 900 μs for elves, to increase the quality of our current reconstruction. We are planning refinements of the on-line TLE-trigger algorithm. To our knowledge, the Auger Observatory is the first and only ground-based facility that measures elves with year-round operation with full horizon coverage, controlled photon counting, and 100 ns resolution. We look forward to possible correlation studies between Auger data and various ongoing experiments: the RELAMPAGO ground-based lightning detection campaign [*Nesbitt et al.*, 2017], the GLM instrument aboard the GOES-16 satellite [*Goodman et al.*, 2013], the ASIM TLE detector [*Neubert et al.*, 2009] and the Mini-EUSO cosmic-ray detector [*Capel et al.*, 2018] aboard the space station, the TARANIS satellite [*Lefeuvre et al.*, 2008], and private ground-based networks such as the GLD-360 of Vaisala, Inc [*Demetriades*, 2012] or the ENTLN of Earth Networks [*Heckman*, 2014]. Any correlation analysis would contribute significantly to atmospheric electricity research.

Acronyms

TLE Transient Luminous Event

elve(s) Emission of Light from Very low frequency perturbations due to Electromagnetic pulse Sources

FD Fluorescence Detector

SD Surface Detector

CCD Charge-coupled device

ISUAL Imager of Sprites and Upper Atmospheric Lightning

CG Cloud-to-Ground

IC Intra-Cloud

EIP Energetic IC Pulses

CID Compact IC Discharges

UHECR Ultra-High Energy Cosmic Rays

UV Ultra-Violet

EMP Electromagnetic Pulse

WWLLN World Wide Lightning Location Network

TLT Third Level Trigger

SLT Second Level Trigger

FLT First Level Trigger

FoV Field of View

IB Initial Breakdown

ADC Analogue to Digital Converter

Acknowledgments

We wish to thank the World Wide Lightning Location Network (http://wwlln.net), a collaboration among over 50 universities and institutions, for providing the lightning location data used in this paper. We acknowledge Robert Marshall for providing one of the most advanced elve simulations to the public, a key tool in understanding the elves observed by the Pierre Auger Observatory.

The successful installation, commissioning, and operation of the Pierre Auger Observatory would not have been possible without the strong commitment and effort from the technical and administrative staff in Malargüe. We are very grateful to the following agencies and organizations for financial support:

Argentina – Comisión Nacional de Energía Atómica; Agencia Nacional de Promoción Científica y Tecnológica (ANPCyT); Consejo Nacional de Investigaciones Científicas y Técnicas (CONICET); Gobierno de la Provincia de Mendoza; Municipalidad de Malargüe; NDM Holdings and Valle Las Leñas; in gratitude for their continuing cooperation over land access; Australia – the Australian Research Council; Brazil – Conselho Nacional de Desenvolvimento Científico e Tecnológico (CNPq); Financiadora de Estudos e Projetos (FINEP); Fundação de Amparo à Pesquisa do Estado de Rio de Janeiro (FAPERJ); São Paulo Research Foundation (FAPESP) Grants No. 2010/07359-6 and No. 1999/05404-3; Ministério da Ciência, Tecnologia, Inovações e Comunicações (MCTIC); Czech Republic – Grant No. MSMT CR LTT18004, LO1305, LM2015038 and CZ.02.1.01/0.0/0.0/16_013/0001402; France – Centre de Calcul IN2P3/CNRS; Centre

National de la Recherche Scientifique (CNRS); Conseil Régional Ile-de-France; Département Physique Nucléaire et Corpusculaire (PNC-IN2P3/CNRS); Département Sciences de l'Univers (SDU-INSU/CNRS); Institut Lagrange de Paris (ILP) Grant No. LABEX ANR-10-LABX-63 within the Investissements d'Avenir Programme Grant No. ANR-11-IDEX-0004-02; Germany – Bundesministerium für Bildung und Forschung (BMBF); Deutsche Forschungsgemeinschaft (DFG); Finanzministerium Baden-Württemberg; Helmholtz Alliance for Astroparticle Physics (HAP); Helmholtz-Gemeinschaft Deutscher Forschungszentren (HGF); Ministerium für Innovation, Wissenschaft und Forschung des Landes Nordrhein-Westfalen; Ministerium für Wissenschaft, Forschung und Kunst des Landes Baden-Württemberg; Italy – Istituto Nazionale di Fisica Nucleare (INFN); Istituto Nazionale di Astrofisica (INAF); Ministero dell'Istruzione, dell'Universitá e della Ricerca (MIUR); CETEMPS Center of Excellence; Ministero degli Affari Esteri (MAE); México – Consejo Nacional de Ciencia y Tecnología (CONACYT) No. 167733; Universidad Nacional Autónoma de México (UNAM); PAPIIT DGAPA-UNAM; The Netherlands – Ministry of Education, Culture and Science; Netherlands Organisation for Scientific Research (NWO); Dutch national e-infrastructure with the support of SURF Cooperative; Poland – National Centre for Research and Development, Grant No. ERA-NET-ASPERA/02/11; National Science Centre, Grants No. 2013/08/M/ST9/00322, No. 2016/23/B/ST9/01635 and No. HARMONIA 5–2013/10/M/ST9/00062, UMO-2016/22/M/ST9/00198; Portugal – Portuguese national funds and FEDER funds within Programa Operacional Factores de Competitividade through Fundação para a Ciência e a Tecnologia (COMPETE); Romania – Romanian Ministry of Research and Innovation CNCS/CCCDI-UESFISCDI, projects PN-III-P1-1.2-PCCDI-2017-0839/19PCCDI/2018, PN-III-P2-2.1-PED-2016-1922, PN-III-P2-2.1-PED-2016-1659 and PN18090102 within PNCDI III; Slovenia – Slovenian Research Agency; Spain – Comunidad de Madrid; Fondo Europeo de Desarrollo Regional (FEDER) funds; Ministerio de Economía y Competitividad; Xunta de Galicia; European Community 7th Framework Program Grant No. FP7-PEOPLE-2012-IEF-328826; USA – Department of Energy, Contracts No. DE-AC02-07CH11359, No. DE-FR02-04ER41300, No. DE-FG02-99ER41107 and No. DE-SC0011689; National Science Foundation, Grant No. 0450696; The Grainger Foundation; Marie Curie-IRSES/EPLANET; European Particle Physics Latin American Network; European Union 7th Framework Program, Grant No. PIRSES-2009-GA-246806; and UNESCO.

References

Aab, A., et al. (2013a), Techniques for measuring aerosol attenuation using the central laser facility at the pierre auger observatory, *Journal of Instrumentation*, *8*(04), P04,009.

Aab, A., et al. (2013b), The Pierre Auger Observatory: Contributions to the 33rd International Cosmic Ray Conference (ICRC 2013).

Aab, A., et al. (2015), The Pierre Auger Cosmic Ray Observatory, *Nuclear Instruments and Methods in Physics Research, Section A: Accelerators, Spectrometers, Detectors and Associated Equipment*, *798*, 172–213, doi:10.1016/j.nima.2015.06.058.

Abraham, J., et al. (2010), The fluorescence detector of the Pierre Auger Observatory, *Nuclear Instruments and Methods in Physics Research Section A: Accelerators, Spectrometers, Detectors and Associated Equipment*, *620*(2-3), 227–251, doi: 10.1016/J.NIMA.2010.04.023.

Allekotte, I., et al. (2008), The surface detector system of the Pierre Auger Observatory, *Nuclear Instruments and Methods in Physics Research Section A: Accelerators, Spectrometers, Detectors and Associated Equipment*, *586*(3), 409–420, doi: 10.1016/J.NIMA.2007.12.016.

Arqueros, F., J. R. Hörandel, and B. Keilhauer (2008), Air fluorescence relevant for cosmic-ray detectionâĂŤSummary of the 5th fluorescence workshop, El Escorial 2007, *Nuclear Instruments and Methods in Physics Research Section A: Accelerators, Spectrometers, Detectors and Associated Equipment*, *597*(1), 1–22, doi: https://doi.org/10.1016/j.nima.2008.08.056.

Baba, Y., and V. A. Rakov (2007), Electromagnetic models of the lightning return stroke, *Journal of Geophysical Research*, *112*(D04102), doi:10.1029/2006JD007222.

Blaes, P. R., R. A. Marshall, and U. S. Inan (2014), Return stroke speed of cloud-to-ground lightning estimated from elve hole radii, *Geophysical Research Letters*, *41*(24), 9182–9187, doi:10.1002/2014GL062392.

Boeck, W. L., O. H. Vaughan, R. Blakeslee, B. Vonnegut, and M. Brook (1992), Lightning induced brightening in the airglow layer, *Geophysical Research Letters*, *19*(2), 99–102, doi:10.1029/91GL03168.

Capel, F., et al. (2018), Mini-EUSO: A high resolution detector for the study of terrestrial and cosmic UV emission from the International Space Station, *Advances in Space Research*, *62*(10), 2954–2965, doi:10.1016/J.ASR.2017.08.030.

Chen, A. B., C. Kuo, Y. Lee, H. Su, R. Hsu, J. Chern, H. U. Frey, S. B. Mende, Y. Takahashi, and H. Fukunishi (2008), Global distributions and occurrence rates of transient luminous events, *Journal of Geophysical Research: Space Physics*, *113*(A8), doi: doi:10.1029/2008JA013101.

Chern, J. L., R. R. Hsu, H. T. Su, S. B. Mende, H. Fukunishi, Y. Takahashi, and L. C. Lee (2003), Global survey of upper atmospheric transient luminous events on the ROCSAT-2 satellite, *Journal of Atmospheric and Solar-Terrestrial Physics*, doi: 10.1016/S1364-6826(02)00317-6.

Cho, M., and M. J. Rycroft (2001), Non-uniform ionisation of the upper atmosphere due to the electromagnetic pulse from a horizontal lightning discharge, *Journal of Atmospheric and Solar-Terrestrial Physics*, *63*(6), 559–580, doi:10.1016/S1364-6826(00)00235-2.

da Silva, C. L., and V. P. Pasko (2015), Physical mechanism of initial breakdown pulses and narrow bipolar events in lightning discharges, *Journal of Geophysical Research: Atmospheres*, *120*(10), 4989–5009, doi:10.1002/2015JD023209.

Demetriades, N. (2012), Advanced lightning warning systems are now available worldwide, *Meteorological Technology International*, pp. 46–48.

Fukunishi, H., Y. Takahashi, M. Kubota, K. Sakanoi, U. S. Inan, and W. A. Lyons (1996), Elves: Lightning-induced transient luminous events in the lower ionosphere, *Geophysical Research Letters*, *23*(16), 2157–2160, doi:10.1029/96GL01979.

Goodman, S. J., R. J. Blakeslee, W. J. Koshak, D. Mach, J. Bailey, D. Buechler, L. Carey, C. Schultz, M. Bateman, E. McCaul, and G. Stano (2013), The GOES-R Geostationary Lightning Mapper (GLM), *Atmospheric Research*, *125-126*, 34–49, doi: 10.1016/J.ATMOSRES.2013.01.006.

Heckman, S. (2014), ENTLN Status Update, in *XV International Conference on Atmospheric Electricity*, pp. 15–20.

Hutchins, M. L., R. H. Holzworth, J. B. Brundell, and C. J. Rodger (2012a), Relative detection efficiency of the World Wide Lightning Location Network, *Radio Science*, *47*(06), 1–9, doi:10.1029/2012RS005049.

Hutchins, M. L., R. H. Holzworth, C. J. Rodger, and J. B. Brundell (2012b), Far-Field Power of Lightning Strokes as Measured by the World Wide Lightning Location Network, *Journal of Atmospheric and Oceanic Technology*, *29*(8), 1102–1110, doi: 10.1175/jtech-d-11-00174.1.

Inan, U. S., Bell, T. F., Rodriguez, and J. V. (1991), Heating and ionization of the lower ionosphere by lightning, *Geophysical Research Letters*, *18*(4), 705–708.

Inan, U. S., C. Barrington-Leigh, S. Hansen, V. S. Glukhov, T. F. Bell, and R. Rairden (1997), Rapid lateral expansion of optical luminosity in lightning-induced ionospheric flashes referred to as 'elves', *Geophysical Research Letters*, *24*(5), 583–586, doi: 10.1029/97GL00404.

Jacobson, A. R., R. Holzworth, J. Harlin, R. Dowden, and E. Lay (2006), Performance Assessment of the World Wide Lightning Location Network (WWLLN), Using the Los Alamos Sferic Array (LASA) as Ground Truth, *Journal of Atmospheric and Oceanic Technology*, *23*(8), 1082–1092, doi:10.1175/JTECH1902.1.

Lefeuvre, F., E. Blanc, J.-L. Pinçon, R. Roussel-Dupré, D. Lawrence, J.-A. Sauvaud, J.-L. Rauch, H. de Feraudy, and D. Lagoutte (2008), TARANIS - A Satellite Project Dedicated to the Physics of TLEs and TGFs, *Space Science Reviews*, *137*(1-4), 301–315, doi:10.1007/s11214-008-9414-4.

Liu, N., J. R. Dwyer, and S. A. Cummer (2017), Elves Accompanying Terrestrial Gamma Ray Flashes, *Journal of Geophysical Research: Space Physics*, *122*(10), 10,510–563,576, doi:10.1002/2017JA024344.

Lyu, F., S. A. Cummer, and L. McTague (2015), Insights into high peak current in-cloud lightning events during thunderstorms, *Geophysical Research Letters*, *42*(16), 6836–6843, doi:10.1002/2015GL065047.

Marshall, R. A. (2012), An improved model of the lightning electromagnetic field interaction with the D-region ionosphere, *Journal of Geophysical Research: Space Physics*, *117*(A03316), doi:10.1029/2011ja017408.

Marshall, R. A., C. L. da Silva, and V. P. Pasko (2015), Elve doublets and compact intracloud discharges, *Geophysical Research Letters*, *42*(14), 6112–6119, doi: 10.1002/2015GL064862.

Marshall, T., W. Schulz, N. Karunarathna, S. Karunarathne, M. Stolzenburg, C. Vergeiner, and T. Warner (2014), On the percentage of lightning flashes that begin with initial breakdown pulses, *Journal of Geophysical Research: Atmospheres*, *119*(2), 445–460, doi:10.1002/2013JD020854.

Mende, S. B., H. U. Frey, R. R. Hsu, H. T. Su, A. B. Chen, L. C. Lee, D. D. Sentman, Y. Takahashi, and H. Fukunishi (2005), D-region ionization by lightning-induced electromagnetic pulses, *Journal of Geophysical Research*, *110*(A11), A11,312, doi:

10.1029/2005JA011064.

Miyasato, R., H. Fukunishi, Y. Takahashi, and M. J. Taylor (2003), Energy estimation of electrons producing sprite halos using array photometer data, *Journal of Atmospheric and Solar-Terrestrial Physics*, *65*(5), 573–581, doi:10.1016/S1364-6826(02)00322-X.

Mussa, R., and G. Ciaccio (2012), Observation of ELVES at the Pierre Auger Observatory, *The European Physical Journal Plus*, *127*(8), 94, doi:10.1140/epjp/i2012-12094-x.

Nesbitt, S. W., P. V. Salio, A. Varble, R. J. Trapp, R. R. Roberts, F. Dominguez, L. Machado, and C. Saulo (2017), Improving high impact weather and climate prediction for societal resilience in Subtropical South America: Proyecto RELAMPAGO-CACTI, *American Geophysical Union, Fall Meeting 2017, abstract #H41K-06*.

Neubert, T., N. B. Crosby, T.-Y. Huang, and M. J. Rycroft (2009), ASIM - an Instrument Suite for the International Space Station, in *AIP Conference Proceedings*, vol. 1118, pp. 8–12, AIP, doi:10.1063/1.3137718.

Newsome, R. T., and U. S. Inan (2010), Free-running ground-based photometric array imaging of transient luminous events, *Journal of Geophysical Research: Space Physics*, *115*(A7), doi:10.1029/2009JA014834.

Rakov, V., and M. Uman (1998), Review and evaluation of lightning return stroke models including some aspects of their application, *IEEE Transactions on Electromagnetic Compatibility*, *40*(4), 403–426, doi:10.1109/15.736202.

Rasmussen, K. L., M. D. Zuluaga, and R. A. Houze (2014), Severe convection and lightning in subtropical South America, *Geophysical Research Letters*, *41*(20), 7359–7366, doi:10.1002/2014GL061767.

Rosado, J., F. Blanco, and F. Arqueros (2014), On the absolute value of the air-fluorescence yield, *Astroparticle Physics*, *55*, 51–62, doi: 10.1016/J.ASTROPARTPHYS.2014.02.003.

Taranenko, Y. N., U. S. Inan, and T. F. Bell (1993), Interaction with the lower ionosphere of electromagnetic pulses from lightning: Heating, attachment, and ionization, *Geophysical Research Letters*, *20*(15), 1539–1542, doi:10.1029/93GL01696.

Valk, F., M. Aints, P. Paris, T. Plank, J. Maksimov, and A. Tamm (2010), Measurement of collisional quenching rate of nitrogen states $N_2(C^3\Pi_u, \mu = 0)$ and $N_2^+(B^2\Sigma_g^+, \mu = 0)$, *Journal of Physics D: Applied Physics*, *43*(385202), doi:10.1088/0022-3727/43/38/385202.

van der Velde, O. A., and J. Montanyà (2016), Statistics and variability of the altitude of elves, *Geophysical Research Letters*, *43*(10), 5467–5474, doi:10.1002/2016GL068719.

Veronis, G., V. P. Pasko, and U. S. Inan (1999), Characteristics of mesospheric optical emissions produced by lightning discharges, *Journal of Geophysical Research: Space Physics*, *104*(A6), 12,645–12,656, doi:10.1029/1999JA900129.

Virts, K. S., J. M. Wallace, M. L. Hutchins, R. H. Holzworth, K. S. Virts, J. M. Wallace, M. L. Hutchins, and R. H. Holzworth (2013), Highlights of a New Ground-Based, Hourly Global Lightning Climatology, *Bulletin of the American Meteorological Society*, *94*(9), 1381–1391, doi:10.1175/BAMS-D-12-00082.1.

Zipser, E. J., D. J. Cecil, C. Liu, S. W. Nesbitt, and D. P. Yorty (2006), Where are the most intense thunderstorms on Earth?, *Bulletin of the American Meteorological Society*, *87*(8), 1057–1071, doi:10.1175/BAMS-87-8-1057.